

---

## REMOVAL OF POLLUTANT TEXTILE DYE FROM AQUEOUS SOLUTION USING MIXED NANOCOMPOSITE OF IRON /ALUMINA OXIDE AND ITS MODIFIED WITH CATIONIC SURFACTANTS

---

Nora M. Hilal\*<sup>1</sup>, O.E. Mostafa<sup>1</sup>

<sup>1</sup>Chemistry Department, Faculty of Science, Al-Azhar University (Girls), Nasr City, Cairo, Egypt.  
[profdrnorahilal@azhar.edu.eg](mailto:profdrnorahilal@azhar.edu.eg), [norahelal832@yahoo.com](mailto:norahelal832@yahoo.com)

---

### ABSTRACT

Nanocomposites of mixed iron/aluminum oxide ( $Fe_2O_3$ .  $Al_2O_3$ ) were prepared by hydrothermal method and modified with a cationic surfactant CTAB for the removal of dye (C.I Acid Orange 67). The morphology and size of the obtained nanocomposites were characterized by SEM, EDX and TEM. The resulting composite and its modified form have been characterized by using the XRD, FT-IR. Batch adsorption experiments were carried out for the removal of acid dye AO67 from aqueous solution. The adsorption of AO67 over the mixed nanocomposite and its modified form were investigated for different parameters such as the effect of CTAB concentration, effect of pH dye solution, effect of initial dye concentration, mass of the adsorbent and the contact time on the adsorption capacity. The adsorption capacities were evaluated using the Langmuir, Freundlich Dubinin- Radushkevich (D-R) and Temkin adsorption isotherm models, the equilibrium experimental data fits perfectly the Langmuir isotherm. Batch kinetic data were analyzed using pseudo first and second order kinetic models, and otherwise different kinetic models. Kinetic data of adsorption are well fitted by the pseudo 2nd order kinetic model with a good agreement with the intra-particle diffusion model. For this the prepared nanocomposite could be regarded as a potential adsorbent for AO67 removal in a wastewater treatment. and were used the optimum conditions for application in the removal of simulated wastewaters dyes (RB222, RY145 and AR37).

**Keywords:** Isotherm, Kinetic, Modified nanocomposites, Hydrothermal route, Acid Dye, CTAB, Waste Water.

### 1. INTRODUCTION

Dyes are the major of the wastewater produced by industries such as textile, paint, cosmetics, etc. The productions of dyes are over 7x10<sup>5</sup> metric tons based on worldwide research and 5 - 10% of the dyes lost in industrial effluents (Bajpai & Jain 2010). Since textile industries consume large quantity of water, the wastewater produced large volume of dyes. Moreover, the type of dyes used in textile industries are synthetic dyes which is toxic dye and cause harm to the aquatic ecosystem (Bajpai & Jain 2012). Other than that, dyes consist of carcinogenic and mutagenic effects which can affect aquatic life and human. The total dye consumption in the textile industry worldwide is more than 10,000 tonnes/year and approximately 100 tones/year of dyes is discharged into water streams (Yagub, *et al.* 2012). Basically, the exact data on the amount of dyes discharged from various processes in the environment are unknown. However, the release of essential amounts of synthetic dyes to the environment has posed challenges to environmental scientists. Various methods such

as adsorption, coagulation, advanced oxidation, and membrane separation are used in the removal of dyes from wastewater (Gupta, 2009). Adsorption is one of the most effective processes of advanced wastewater treatment which industries employ to reduce hazardous inorganic/organic pollutants present in the effluent (Kant, 2012). Several methods have been used for the removal of dyes from the aquatic environment, including physical, chemical, and biological processes. Among these methods, adsorption is a widely used for dye removal from wastewaters (Bhattacharyya and Sharma, 2005).

Nanotechnology promises the possibility of creation of nanostructures of metastable phase with non-conventional properties including super conductivity and magnetism. The materials in the nanometer scale exhibit properties distinctively different from that of bulk due to quantum size effects and the occurrence of large amounts of surfaces and interfaces because of their reduced size in nanometer scale this different from the materials in micrometer scale (Ventura, *et al.*

2004). Thus, the materials having three-dimensional network consisting of at least two phases with one dispersed in another i.e., matrix are known as nanocomposites. Many of the nanocomposites are synthesized via various synthetic routes such as sol-gel synthesized CdO-ZnO nanocomposite are used in gas sensing (Karami, 2010). Apart from the various nanocomposites prepared having characteristics application nanocomposites of alumina and iron oxide are of great importance.  $\text{Al}_2\text{O}_3$  is amphoteric in nature and due to its hardness, it is used as an abrasive and due to its high melting point is used as a refractory material. It has a high thermal conductivity for ceramic material instead of being an electrical insulator. Corundum is the most common form of crystalline alumina and the alpha and gamma phase of  $\text{AlOOH}$  are commonly known as Diaspore and Boehmite respectively (Kim, *et al.* 2007). Alumina is also used as filler in plastics, as catalysts (Alvarez, *et al.* 2008), again they are widely used for the removal of water from gas stream and alumina acts as a very good adsorbent as well. Iron oxides are considered as one of the most important transition metal oxides. These oxides have huge applications as adsorbents (Yu, *et al.* 2008), catalysts (Faraji, *et al.* 2010), sorbents, pigments, flocculants, coatings, gas sensors (Arshak & Gaidan 2005) ion exchangers and as lubricants. Iron oxide nanocomposite has various potential applications in the areas of magnetic recording, magnetic data storage devices, toners, magnetic resonance imaging, waste water treatment, bioseparation, medicines etc. Hydrothermal Synthesis is a method used for the preparation of fine powders of ceramic oxides which involves the exploitation of the properties of water under high pressure and temperature. Thus, hydrothermal technique has been a very effective route for the preparation of nanoscale ceramic oxides like iron oxide and alumina (Nalwa, 2009 and Akazdam, S. *et al.*, 2017). Mixed nanocomposite modified with a cationic surfactant CTAB surfactant (Cetyl Trimethyl Ammonium Bromide) has shown very high adsorption capacity for anionic dye (Sudipta, *et al.* 2009 and Rajabi, A.A. *et al.*, 2016). In this study the adsorption method was

carried out by using mixed nanocomposite (MNC) and its modified by a cationic surfactant CTAB surfactant (MMNC) as synthesis chemical adsorbent for removal of C.I. Acid Orange 67 from aqueous solution and were used the optimum conditions for application in the removal of simulated wastewaters dyes (RB222, RY145 and AR37).

## 2. MATERIALS AND METHODS

### 2.1. Materials

All chemicals used in this study were of analytical grade.  $\text{Al}(\text{NO}_3)_3 \cdot 9\text{H}_2\text{O}$  and  $\text{FeSO}_4 \cdot 7\text{H}_2\text{O}$ ,  $\text{NH}_3$  solution and NaOH were supplied from Aldrich Company, Acid dye, nylomine orange (C.I. Acid Orange 67) was supplied from Imperial Chemical Industries, ICI, and cetyl trimethyl ammonium bromide, CTAB (S.D. Fine Chem. Ltd). All chemicals were used without further purifications. Bidistilled water was used throughout the experiments for preparation and dilution of the solutions.

### 2.2. Preparation of nanocomposites composed of mixed iron and aluminum oxide (Adsorbent) and modification by cetyl trimethyl ammonium bromide, CTAB

Nanocomposites of mixed iron/ aluminium oxide were prepared by hydrothermal method. The  $\text{Al}(\text{NO}_3)_3 \cdot 9\text{H}_2\text{O}$  and  $\text{FeSO}_4 \cdot 7\text{H}_2\text{O}$  salts were taken in a molar ratio of 1:1 and were mixed in a 50 ml distilled water. Then the mixed solution is stirred vigorously. Then a mixed precipitant was prepared by adding 25ml of 2M  $\text{NH}_3$  solution into 25 ml of 2 M NaOH solution to maintain a ratio of 1:1. The mixed precipitant was added drop wise to above mixture solution with vigorous stirring. Simultaneously the pH of the solution was measured using pH meter. At pH 5.6 green precipitate was formed. After the formation of precipitate the whole mixture solution was transferred to 100 ml Teflon lined pressure pot. The pressure pot was sealed and kept in an electric oven at  $180^\circ\text{C}$  for 6 h. After that the autoclave was cooled at room temperature and the resultant product was centrifuged, washed with deionized water several times and dried at  $50^\circ\text{C}$  for 5-6 h followed by grinding. Further it

was calcined at both 500°C and 1000°C, which was found to be reddish brown in color, and was assumed to be Fe<sub>2</sub>O<sub>3</sub> - Al<sub>2</sub>O<sub>3</sub> nanocomposite.

Surfactant CTAB selected as modifying agent, stock surfactant solution was prepared from surfactant at 1% (wt/v) concentration. The modification process carried out by mixing 2g of alumina- iron oxide as adsorbent in 100 ml of different concentration from 1% CTAB are 0.01%, 0.02%, 0.03%, 0.04% and 0.05% (Rouf, *et al.* 2015), then shaking this solution on shaker at a constant agitation speed (200rpm) for 1h, then the solution filtered and product of modified nanocomposite was dried at 50°C until constant weight was reached and stored for further investigation.

The surface morphology of iron oxide–alumina mixed nanocomposite was characterized by using Scanning electron microscope, SEM (JEOL JSM-5400 SEM - Tokyo, Japan,) and was operated at 20 kV. In order to increase the conductivity of the samples, they were gold coated using a JEOL FRC 1200 fine coater before taking SEM. The powder X-ray diffraction patterns were obtained on a Pan analytical X-ray diffractometer (PW1830). Transmission electron microscope (TEM) measurements were performed using (JEOL JEM-1010 - Tokyo, Japan) with resolution point 0.45nm was used to characterize the iron oxide–alumina mixed nanocomposite materials and was operated at 200 kV. The mixed nanocomposites were dispersed in ethanol and then a drop of the above dispersion was taken on a carbon coated copper grid (300 meshes) for TEM imaging. Fourier transform infrared (FTIR) spectroscopy was used in order to analysis and detects the functional group which present in sample before and after adsorption process. FTIR spectra were recorded on Mattson 1000, Unicam infrared spectrophotometer, Cambridge, England in the range 400–4000cm<sup>-1</sup> using KBr pellets. A dry constant weight from each composite was ground with 2 g of KBr and then pressed to form transparent disks. The powder X-ray diffraction patterns were obtained on a Pan

analytical X-ray diffractometer (PW1830). The zero-point charge of iron oxide–alumina mixed nanocomposite was determined by a digital pH meter (Satorius Model PB-11) combined with glass electrode and was used for other all experiments. A UV-visible spectrophotometer (Model T60 spectrophotometer, United Kingdom) was used for adsorption study of C.I. Acid Orange 67.

### 2.3. Batch Adsorption Studies.

The effect of various parameters on the removal of C.I. Acid Orange 67 onto iron oxide–alumina mixed nanocomposite was studied. For each experimental run, 40 ml of dye solutions of known initial concentration and pH were taken in 100 ml plugged conical flask. A suitable adsorbent dose of iron oxide alumina mixed nanocomposite was added to conical flasks containing 40 mL dye solutions, adsorption of dye solutions was carried out at 25±1°C for 24 h in batch system and the mixture was shaken at a constant agitation speed (200 rpm) for 30 min. After shaking, the suspension was separated from the adsorbent by centrifugation at a rotation speed of 6000 r/min for 5 min. Adsorption equilibrium isotherms were studied using iron oxide alumina mixed nanocomposite dosages from (0.02-0.4 g) per 40 ml of dye solutions. Initial concentrations were ranged from (5-150 mg/L) using initial pH 5.9±0.5 which lowers than zero point charge (pH<sub>ZPC</sub>) of the adsorbent, the solution was separated from the mixture and analyzed for AO67 concentration. The amount of dye adsorbed per unit mass of the adsorbent was analyzed by UV visible spectrophotometer and calculated as follows (Muntean, S.G.2018):

$$q_e \text{ mg/g} = \frac{(C_o - C_e)V}{M} \quad (1)$$

and the percent removal may be calculated as:

$$\text{Removal\%} = \left( \frac{(C_o - C_e)}{C_o} \right) 100 \quad (2)$$

Where C<sub>o</sub> is the initial concentration (mg/ L) and C<sub>e</sub> is the dye concentration (mg/L) at any time, V is the volume of the solution (ml) and M is the weight of the adsorbent used (g). The

effect of pH on the rate of adsorption was investigated using dye concentration of 100 mg/L for constant iron oxide–alumina mixed nanocomposite dosages. The pH values were adjusted with 0.5N HCl and 0.5N NaOH solutions. The suitability of the Langmuir, Freundlich Dubinin- Radushkevich (D-R) and Temkin adsorption models to the equilibrium data were investigated for dye sorbent system.

### 3. RESULT AND DISCUSSION

#### 3.1. Characterizations of Synthesis Nanocomposites and its modified.

##### 3.1.1. Structural Analysis of Mixed Alumina/Iron Oxide Nanocomposite by XRD Analysis

Figure 1 the XRD pattern indicates the crystal structure of mixed alumina/iron oxide nanocomposite particles, where the peak at  $2\theta = 33.45^\circ$  is corresponding to iron oxide phase JCPDS card (19-0629) and that at  $2\theta = 38.7^\circ, 44.62^\circ, 52.8^\circ$  and  $68.8^\circ$  are corresponding to  $\text{Al}_2\text{O}_3$  JCPDS card (10-173). It is obvious that these peaks appear broader indicating smaller crystallite size of the produced mixed alumina/iron oxide nanocomposite particles than that of the starting particles and this may be devoted to the method of preparation of the composite which cause dispersion of alumina particles. The crystallite size of both phases of produced composite can be calculated from peaks at  $2\theta = 33.45^\circ$  corresponding to  $\text{Fe}_2\text{O}_3$  phase and peak at  $2\theta = 44.62^\circ$  corresponding to  $\text{Al}_2\text{O}_3$  phase using Sherrer Equation (3).

$$L_\theta = \frac{K\lambda}{\beta \cos \theta} \quad (3)$$

Where  $\beta$  is the full width at half maximum FWHM of diffraction peak,  $\lambda$  is the wave length of X-ray (0.154 nm),  $L_\theta$  is the crystallite size, and  $\theta$  is the Bragg peak position. The crystallite size was found to be 28.33 nm and 22.45 nm for both  $\text{Al}_2\text{O}_3$  and  $\text{Fe}_3\text{O}_4$  respectively.

##### 3.1.2. Structural Analysis of Mixed Alumina/Iron Oxide Nanocomposite by Transmittance FTIR Spectra.

Figure (2a, b) represent the FTIR spectra of mixed nanocomposite (MNC) compared with FTIR spectra of modified mixed nanocomposite with cationic surfactant (CTAB). The spectra show the deformation of water molecules at  $1648.84 \text{ cm}^{-1}$  and O–H bending vibrations appear. Strong band are observed at  $1359 \text{ cm}^{-1}$  due to Al–O bond vibrations in the  $\text{Al}_2\text{O}_3$ . The peak around  $1115.62 \text{ cm}^{-1}$  corresponds to the Fe–O stretching vibration of  $\text{Fe}_2\text{O}_3$  phase. The bands at  $1115.62 \text{ cm}^{-1}$  and  $616 \text{ cm}^{-1}$  appear due Al–O bonds (Tsai, et al. 2005). The spectra revealed that O–H vibrations  $3456 \text{ cm}^{-1}$  due to the water in the lattice (Srivastava, et al. 2011) and O–H bending vibrations appear at  $1648.84 \text{ cm}^{-1}$ . Further the bands at  $1359 \text{ cm}^{-1}$  corresponds to = CH in-plane vibrations and  $616 \text{ cm}^{-1}$  corresponding to - CH out-of-plane vibrations. From FT-IR analysis it is observed that the sample is a mixed composite of iron -alumina

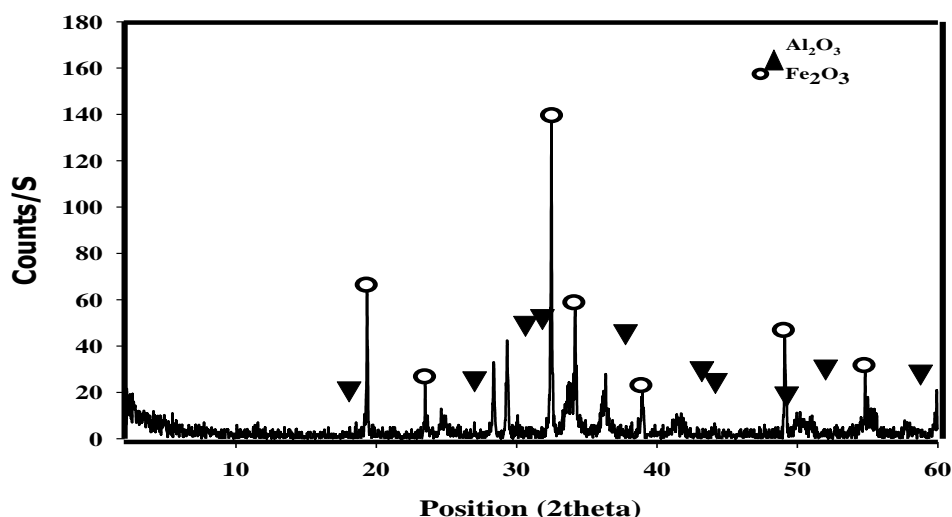


Figure (1): XRD data of Mixed Alumina/Iron Oxide Nanocomposite.

oxide. The Figure (2b) represent the FTIR spectra for the modification of iron -alumina oxide (MNC) nanocomposite with cationic surfactant (CTAB). The peak at 1380 cm<sup>-1</sup> is attributed to C-N band and the peaks at 2885 and 2925 cm<sup>-1</sup> are attributed to different C-H bands vibration of CTAB.

**3.1.3. Morphology Analysis of Mixed Alumina/Iron Oxide Nanocomposite and its modified (SEM, Mapping Scan, Elemental detection X- ray and TEM Analysis):**

The SEM, EDAX and mapping scan images of mixed nanocomposites (mixed alumina/iron oxide nanocomposite) obtained by hydrothermal synthesis and its modified with

CTAB of as-prepared. It is observed from the SEM images, photo 1 (a, b) that the as-prepared samples are rod shaped and are in the size range of 20–100 nm. EDAX figures of mixed nanocomposites and its modified were shown in Figures 3 (a, b). The presence of Fe, Al and O elements in the mixed nanocomposite were confirmed by the EDAX spectrum Figure (3a) and the presence of elements of N, C and Br which confirmed the modification of (MNC) with (CTAB) and represent by Figure (3b). Photo (2), represent the maps of elements of iron (a) and aluminum (b) which show the distribution and homogeneity of elements in sample of nanocomposite.

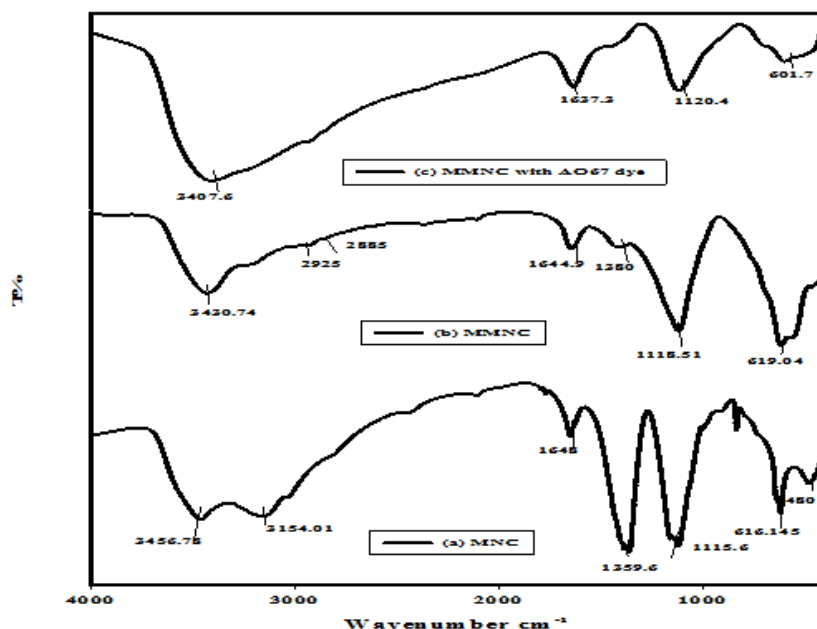


Figure (2): (a) FTIR spectra of mixed nanocomposite of iron/alumina oxide(MNC), (b) FTIR spectra of its modified (MMNC) and (c) (MMNC) after acid orange 67dye adsorption.

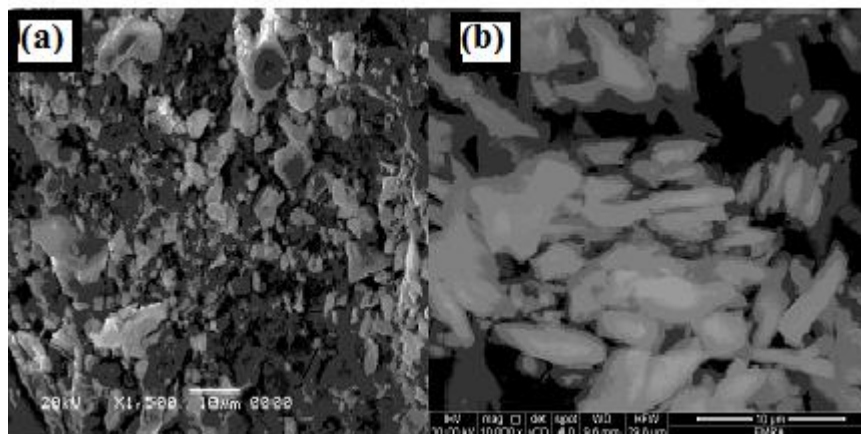


Photo (1):( a) SEM of iron oxide–alumina mixed nanocomposite(MNC) , (b): SEM of modified iron oxide–alumina mixed nanocomposite with CTAB(MMNC).

Transmission electron microscope (TEM) was used to obtain more information about the formation, morphology and dimensions of mixed oxide nanocomposite, we have carried out the TEM imaging. Photo (3) Shows the TEM micrograph of  $\text{Fe}_2\text{O}_3\text{-Al}_2\text{O}_3$  mixed oxide nanocomposite. It was observed from the TEM imaging that the nanoparticle formed were not having uniform size; instead a size ranges from 20–100 nm was found. The produced composite showed approximate uniform spherical nanoparticles, the magnetite nanoparticles are finally divided and well distributed within the composite as shown in Photo (3a). It was not possible to distinguish between the iron oxide and aluminum oxide

phase's structure. Photo (3b) shows the selected area diffraction pattern of mixed oxide nanocomposites. The corresponding diffraction rings and bright spot on the electron diffraction pattern indicate the formation of highly crystalline  $\text{Fe}_2\text{O}_3\text{-Al}_2\text{O}_3$  mixed oxide nanocomposite, which is also consistent with XRD results.

### 3.1.4. Zero Surface Charges -The Characteristic Analysis of Mixed Alumina/Iron Oxide Nanocomposite.

The influence on the solution pH on the dye uptake can be explained on the basis of the pH zero-point charge or isoelectric point of the adsorbent. The value of the pH necessary to affect a net zero charge on a solid surface in the

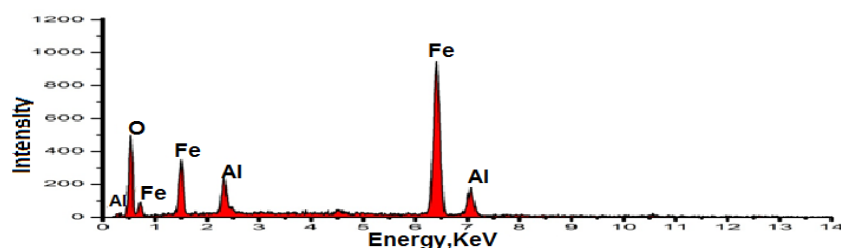


Figure (3a). EDAX spectrum of iron oxide–alumina mixed nanocomposite.

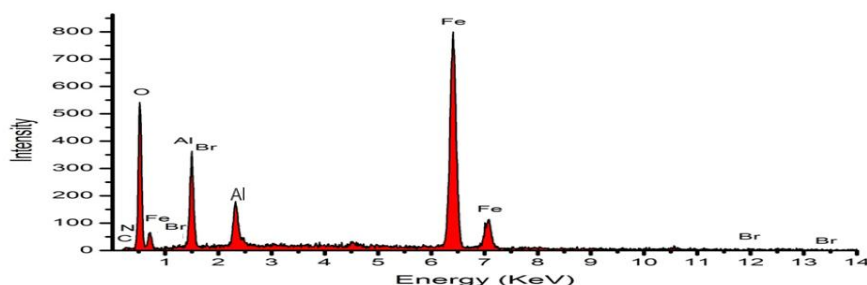


Figure (3b): EDX for of iron oxide–alumina mixed nanocomposite treatment with CTAB.

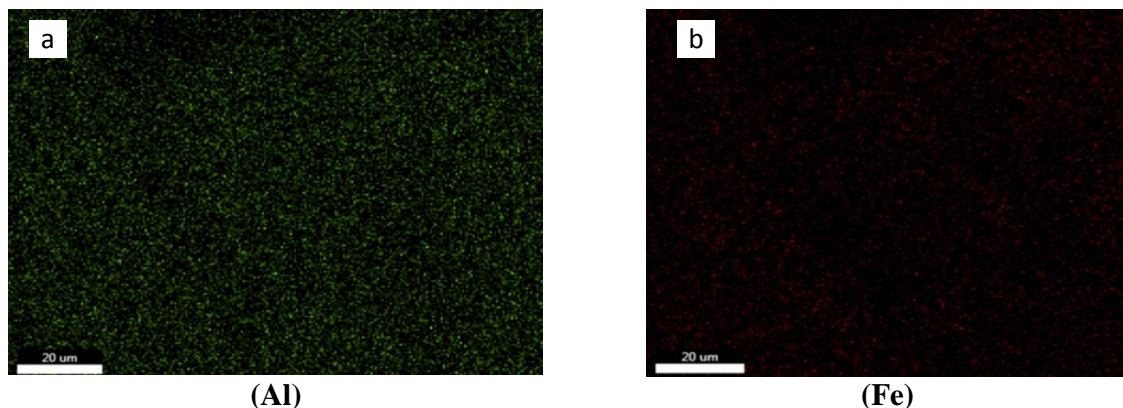


Photo (2): Maps of elements (a) for Iron and (b) for Aluminum

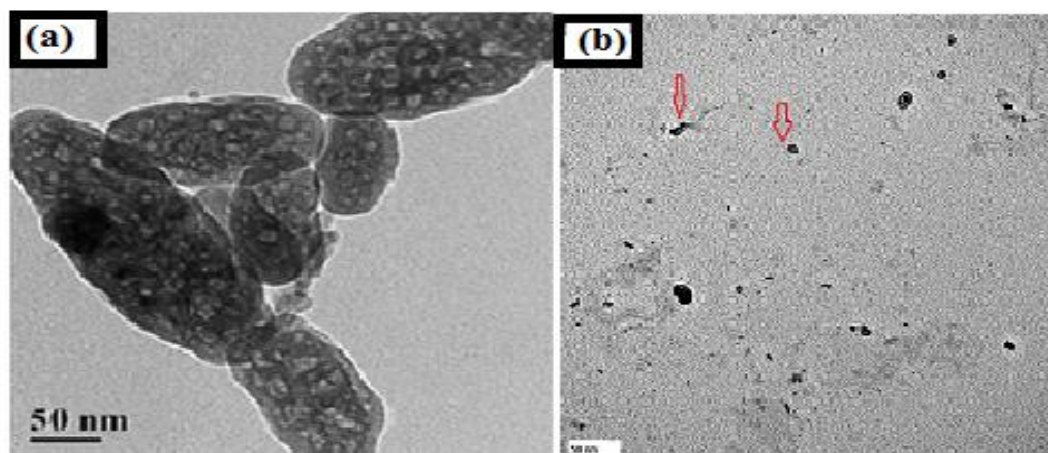


Photo 3 (a, b): TEM micrograph of iron oxide–alumina mixed nanocomposite.

absence of specific sorption is called the point of zero charge,  $pH_{ZPC}$ . The zero-surface charge of iron oxide–alumina mixed nanocomposite was determined by using the solid addition method (Hamid, *et al.* 2016 and Hashemian, 2010). The experiment was conducted in a series of 250 mL glass stoppard flasks. Each flask was filled with 50 mL of different initial pH 0.01N  $KNO_3$  solutions and 0.1 g of mixed nanocomposite. The pH values of the  $KNO_3$  solutions were adjusted between 2 to 10 by adding either 0.1 M HCl or 0.1 M NaOH. The suspensions were then sealed and shaken for 48 h at 150 rpm. The final pH values of the supernatant liquid were noted. The difference between the initial pH ( $pH_o$ ) and final pH ( $pH_f$ ) values ( $\Delta pH = pH_o - pH_f$ ) was plotted against the values of  $pH_o$ . The point of intersection of the resulting curve with abscissa, gave the  $pH_{ZPC}$ .

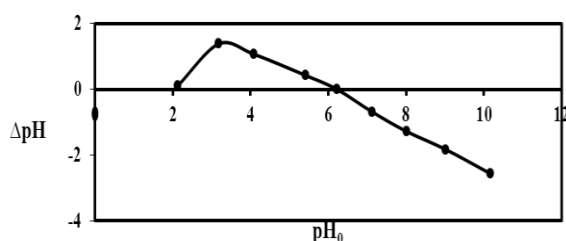
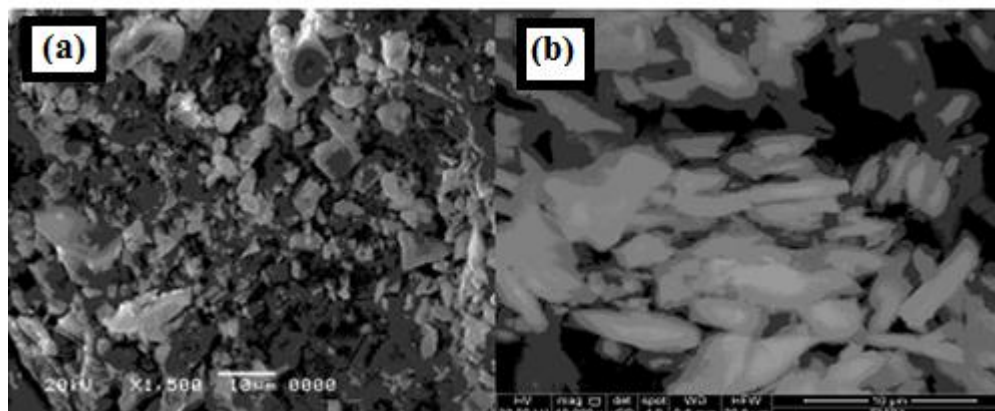


Figure (4): Zero-point charge of mixed alumina/iron oxide nanocomposite.

Figure 4 shows that the plot between  $\Delta pH$ , i.e. ( $pH_o - pH_f$ ) and  $pH_o$  for  $pH_{ZPC}$  measurement for iron oxide/alumina mixed nanocomposite. The point of zero charge is found to be 6.22. At a low pH ( $< pH_{ZPC}$ , i.e.  $< 6.22$ ), the iron oxide/alumina mixed nanocomposite surface has positive charge, and the Acid Orange -67 dye molecules, with a sulfuric group ( $SO_3$ ), have a negative charge (Aharoni & Sparks 1991), attracting the iron oxide–alumina mixed nanocomposite particles. Thus, the degradation reaction between the dye molecules and could mixed alumina/iron oxide nanocomposite be achieved easily.

### 3.1.5. Changing the morphology of Mixed Alumina/Iron Oxide Nanocomposite and its modified by adsorption of C.I. Acid Orang 67.

Photo 4 (a, b) shows adsorption of AO67 dye on MNC and its modified MMNC surfaces. The cluster of an AO67 dye is shown on the surface of adsorbent. The AO 67 dye is adsorbed in microspores and mesoporous of adsorbent mixed alumina/iron oxide nanocomposite. The presence of Fe, Al and O elements with S, N and Na elements in Figure (5) represent by EDX spectrum was confirmed the attraction between the mixed nanocomposite and AO67.



**Photo 4 :** SEM of mixed alumina/iron oxide nanocomposite(a) and its modified(b) loaded with AO67.

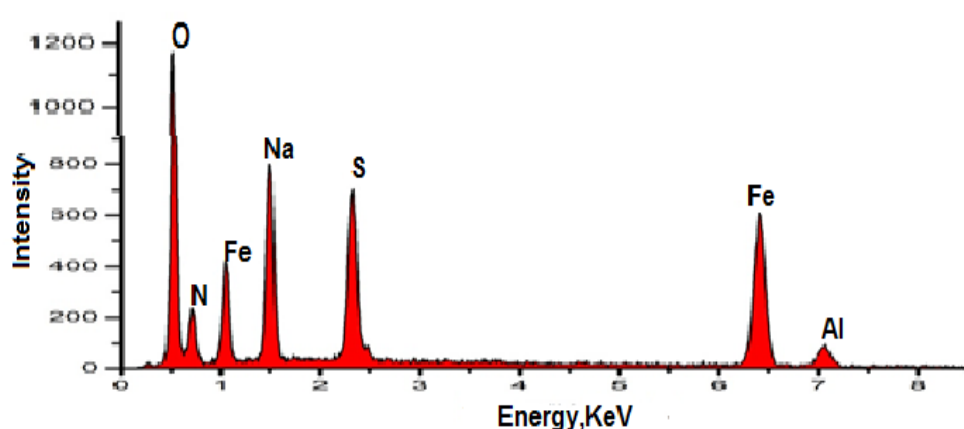


**Figure (5) :** EDX spectrum of mixed alumina/iron oxide nanocomposite with dye AO 67.

The FT-IR spectrum of mixed composite of iron /Alumina oxide and its modified which are loaded with AO 67 dye represents by Figure (2a, b and c) overall figures shows some shift as well as changes in the intensity of peaks compared to mixed composite of iron /Alumina oxide and the results show that AO67 has been successfully attachment in the mixed composite and its modified (MMNC). The strong band at  $1359\text{ cm}^{-1}$  which confirmed the presence of Al-O disappeared in the result sample and the band represent the Fe-O shifted to higher value these confirmed the successfully attachment of dye with mixed nanocomposite and its modified (MMNC).

### 3.2. Structural characterizations of Acid dye AO 67

The water-soluble Acid Orange 67 dye which has the following characters:

### 3.3. Adsorption study of Acid dye AO 67 by mixed nanocomposites and its modified

#### 3.3.1. Summarize the effects interaction of adsorption parameters on the percentage removal of dye by MNC and MMNC as adsorbents

The results obtained from 3D experimental runs conducted to observe the effect of the four adsorption factors (solution pH, initial dye concentration, adsorbent dose and time) using MNC and MMNC. The analyses are supported by the 3D plots of the interaction effects of the four factors on the percentage removal of dye.

### 3.3.1.1. The interaction effect of pH solution and initial dye concentration

Figure (9), represent the combined effect of the solution pH and dye concentration. Suggests that increasing dye concentration results in an increasing removal of the dye, whereas, it increases with decreasing the pH value. Ascending trend in dye uptake with decreasing pH may be attributed to the positive charges on the dye molecules in the acidic medium, from figure it can be seen that at low pH value ( $\text{pH} < 5.42$ ) more than 79% of initial dye percent in the solution was removed onto MNC adsorbent and ( $\text{pH} < 8.5$ ) more than 99% onto MMNC adsorbent. While the increase in the solution pH ( $\text{pH} > 5.42$  or  $> 8.5$ ) with increase in the initial dye concentration resulted in significance reduction in the percentage removal. The presence of these positively

charged functional groups will also increase the percentage removal due to the attraction of the negatively charged dye ions by the positively charged surface functional groups and the trend reverses when the dye adsorption decreases with increasing concentration. This behavior can be understood as the increasing adsorbate concentration with fixed adsorbent dose would result in saturation of the binding sites on the surface and subsequently declining of the adsorbate uptake with increasing concentration.

### 3.3.1.2. The interaction effect of solution pH and adsorbent dose

The effect of pH and adsorbent dose on dye removal onto MNC and MMNC is shown in 3D plot (Figure 10). Percent removal increased with increasing adsorbent dose and decreasing pH. At lower pH ( $\text{pH} < 5.42$ ) more than 79% and at pH ( $\text{pH} < 8.5$ ) more than 99 % of dye was

**Table (1): Some of physical properties of C.I. Acid Orange 67.**

<b>Commercial name</b>	nylomine orange
<b>IUPAC name:</b>	Sodium 4-[3-[2-methyl-4-(4-methylphenyl) sulfonyloxyphenyl] diazenylanilino]-3-nitrobenzenesulfonate
<b>Other names</b>	Acid Orange 3R, Acid Orange ARG, Euramina Orange 3RL, Nylanthrene Yellow C 3RL and Nylosan Yellow N-3RL.
<b>Molecular formula</b>	$\text{C}_{26}\text{H}_{21}\text{N}_4\text{NaO}_8\text{S}_2$
<b>Type</b>	Anionic
<b>Molecular Structure</b>	Single azo class
<b>Molecular weight</b>	604.59
<b>CAS Registry number</b>	12220-06-3
<b>Appearance</b>	Orange red powder
$\lambda$ max.	442 nm
<b>Structure formula</b>	

removed onto MNC and MMNC respectively, this result showed the significance of solution pH on the adsorption process of dye ions, the maximum percentage removal was predicated at solution (pH > 5.42 or > 8.5). Such behavior justified by the presence of large quantity of positively charged surface functional groups at lower solution pH and large amount of adsorbent dose (0.3 g /40 ml of dye).

**3.3.1.3. The interaction effect of solution pH and contact time**

The 3D surface plot for combined effect of pH and contact time. Figure (11) shows at lower pH, the dye removal increases with increasing contact time as the time of

adsorption increases, dye % removal increase. This result indicates that both adsorption factors have significant effect on the % removal of dye.

**3.3.1.4. The interaction effect of adsorbent dose and initial dye concentration**

The combined effect of adsorbent dose and initial dye concentration on removal dye in 3D surface plot is shown in Figure (12). It may be noted that the dye removal increased with increasing adsorbent dose and increasing dye concentration. This is due to increase in initial dye concentration, adsorption sites, surface area of the adsorbent are saturated, resulting in decrease in the adsorption efficiency.

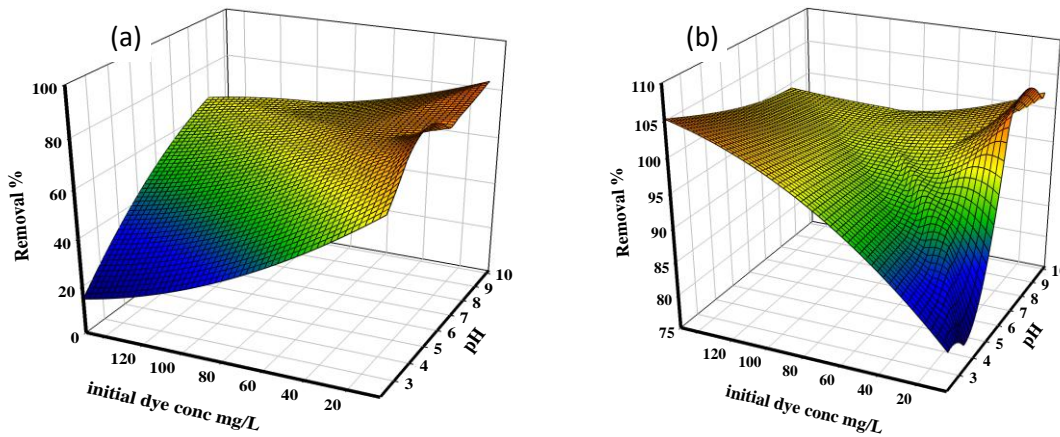


Figure (9): 3D plot of the interaction effect of solution pH and initial dye concentration on adsorption of AO67 onto (a) MNC and (b) MMNC.

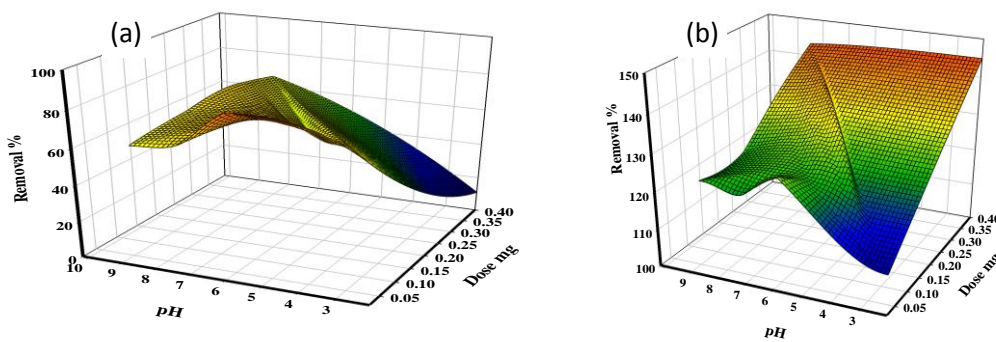
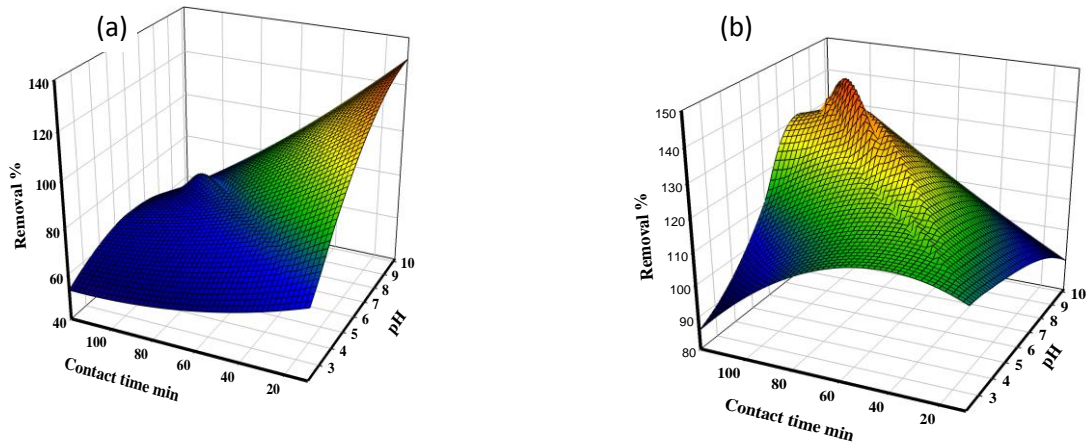


Figure (10): 3D plot the interaction effect of solution pH and adsorbent dose on adsorption of AO67 onto (a) MNC and (b) MMNC.

**3.3.1.5. The interaction effect of initial dye concentration and contact time**

The interactive effect of initial dye concentration and contact time on dye removal is shown in 3D surface plot in Figure (13). However, beyond time 85 and 65 min of MNC

and MMNC respectively, increasing the adsorption time has no considerable improvement in % dye removal. This is due to an equilibrium stage the adsorption achieves its saturation, possibility no further adsorption occurs, and the contact time has no longer effect on % removal of dye.



**Figure (11): 3D plots the interaction effect of pH of solution and contact time on adsorption of AO67 onto (a) MNC and (b) MMNC.**

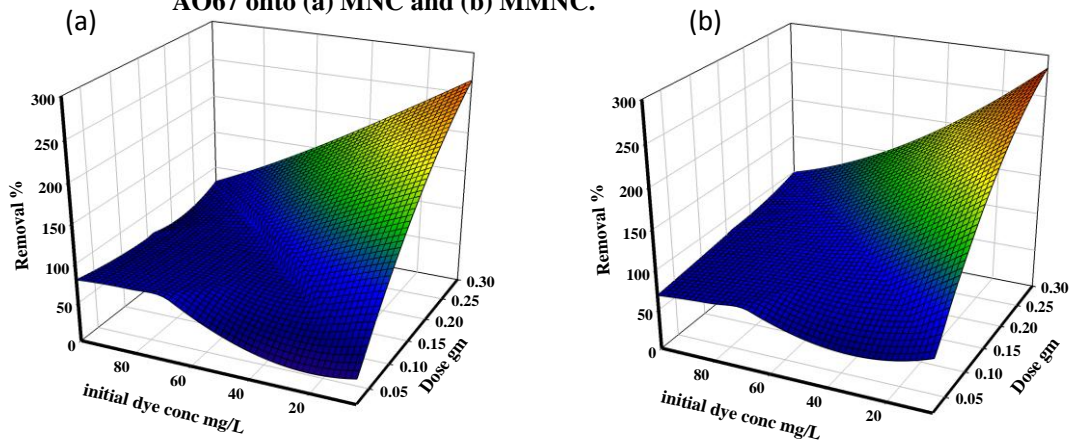


**Figure (12): 3D plots the interaction effect of adsorbent dose and initial dye concentration on adsorption of AO67 onto (a) MNC and (b) MMNC.**

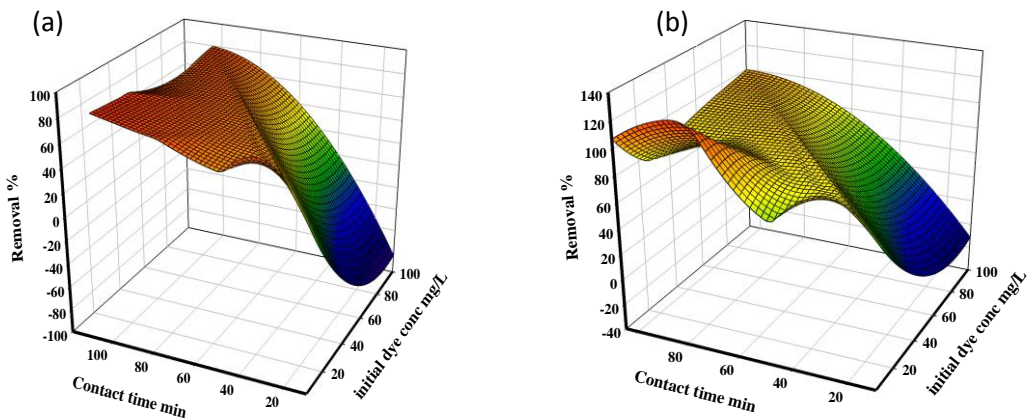


**Figure (13): 3D plot the interaction effect of contact time and initial dye concentration on adsorption of AO67 onto (a) MNC and (b) MMNC.**

### 3.3.1.6. The interaction effect of adsorbent dose and contact time

Figure (14) shows the interactive influence of adsorbent dose and contact time on the dye removal from aqueous phase. It is evident that the dye removal increased with the increase in both the adsorbent dose and contact time. The observed trend may be understood the increase in adsorbent dose would make higher number of adsorption sites available.

### 3.3. Applicability of various adsorption isotherm models on dye adsorption.

The adsorption isotherm is significant for the explanation of how the adsorbent will interact with the adsorbate and give an idea of adsorption capacity. They play an important role in understanding the mechanism of adsorption. The surface phase may be considered as a monolayer or multilayer. Several isotherm models are presented in the literature (Seeds, 2011). In this work, the equilibrium data for AO67 on iron oxide–alumina mixed nanocomposite (MNC) and (MMNC) were modeled with the Langmuir, Freundlich and Temkin models. Langmuir and Freundlich models are the most widely used to describe the adsorption isotherm.

The Langmuir isotherm is valid for adsorption of a solute from a liquid solution as monolayer adsorption on a surface containing a finite number of identical sites. Langmuir isotherm model assumes uniform energies of adsorption onto the surface without

transmigration of adsorbate in the plane of the surface (Langmuir, 1916). Therefore, the Langmuir isotherm model was chosen for estimation of the maximum adsorption capacity corresponding to complete mono-layer coverage on MNC and MMNC surfaces. The experimental data are analyzed according to the linear form of the Langmuir isotherm equation. The linear Langmuir isotherm equation is represented by the following equation:

$$\frac{C_e}{q_e} = \frac{C_e}{q_{\max}} + \frac{1}{k_L q_{\max}} \quad (4)$$

Where,  $C_e$  is the equilibrium concentration (mg/L),  $q_e$  is the amount adsorbed at equilibrium (mg/g).  $q_m$  and  $k_L$  are Langmuir constants related to the adsorption efficiency and energy of adsorption, respectively (Patil, 2014). The linear plots of versus suggest the applicability of the Langmuir isotherms for the removal of AO67 dye onto MNC and MMNC. The values of  $q_m$  and  $k_L$  of linear expression of Langmuir adsorption isotherm was calculated from the slopes and intercept of the linear plot of  $C_e / q_e$  versus  $C_e$  and are shown in Figures (15 a,b and c). The results of correlation coefficients predicted from this model for the removal of AO67 dye by MNC and MMNC are represented in Table (2). The correlation coefficients reported in the table showed strong positive evidence on the adsorption of the dye onto the adsorbent follows the Langmuir isotherm represents the best fit of experimental data.

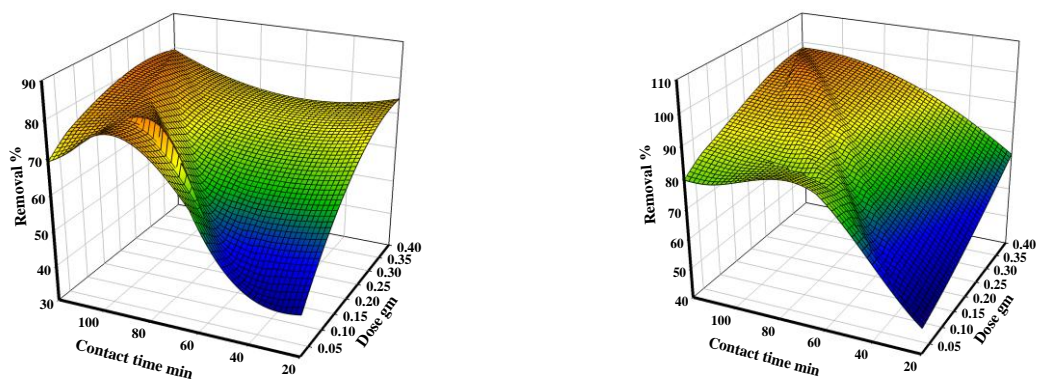


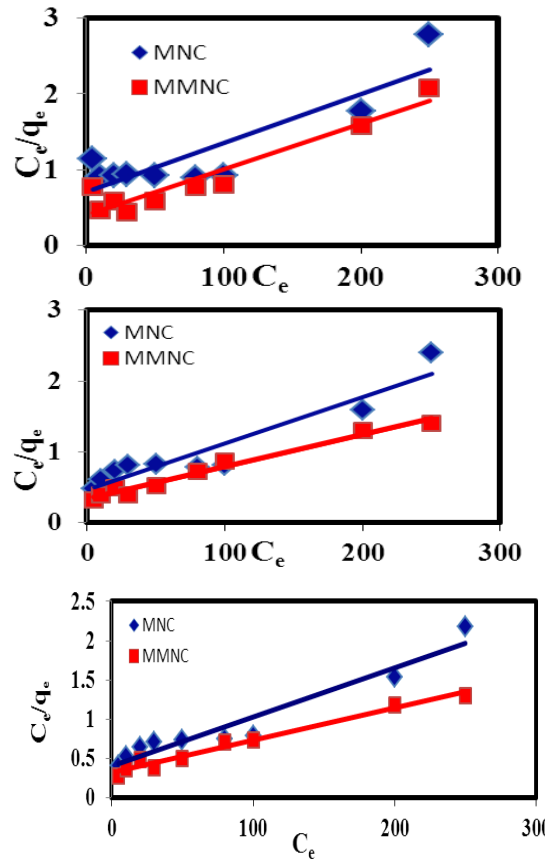
Figure (14): 3D plot the interaction effect of contact time and adsorbent dose on adsorption of AO67 onto (a) MNC and (b) MMNC.

The applicability of the linear form of Langmuir isotherm model to AO67 was proved by the high correlation coefficients  $R^2 > 0.99$ . This suggests that the Langmuir isotherm provides a good model of the dye adsorption system. The fact that Langmuir isotherm fits the experimental data very well confirms the monolayer coverage of dye onto MNC and MMNC and the homogeneous distribution of active sites on the adsorbent, since the Langmuir equation assumes that the surface is homogeneous (Dakhil, 2013). The essential features of the Langmuir isotherm can be expressed in terms of a dimensionless constant called separation factor  $R_L$  also called equilibrium parameter which is defined by equation (5). The value of  $R_L$  indicates the shape of the isotherms to be either unfavorable ( $R_L > 1$ ), linear ( $R_L = 1$ ), favorable ( $0 < R_L < 1$ ) or irreversible ( $R_L = 0$ ) (Seeds, 2011).

$$R_L = \frac{1}{(1 + k_L C_0)} \tag{5}$$

Where,  $C_e$  (mg/L) is the initial dye concentration and  $R_L$  (L/mg) is the Langmuir constant related to the energy of adsorption. The influence of isotherm shape on whether adsorption is favorable or unfavorable has been considered. For a Langmuir type adsorption process, the isotherm shape can be classified by a dimension less constant separation factor  $R_L$ , given by equation (5). The calculated values at different initial AO67 dye concentrations are represented in Table (2). It was found to be between 0 and 1 for AO67 suggesting the isotherm to be favorable at the concentrations studied. The degree of favorability is generally related to the irreversibility of the system, giving a qualitative assessment of the MNC-AO dye interactions. The degrees tended toward zero (the completely ideal irreversible case) rather than unity (which represents a completely reversible case).

The Freundlich ,Temken and D-R Dubinin-Radushkevich isotherm models were also an important relationship describing the sorption of solutes from a liquid to a solid surface. The calculated constants of each methods were collected in Table 2



Figures (15a,b and c): The Langmuir isotherm model by (MNC and MMNC ) at 25 ,40 and 60°C

### 3.4. Adsorption kinetics

Kinetic models have been used to investigate the mechanism of sorption and potential rate controlling steps, which is helpful for selecting optimum operating conditions for the full-scale batch process. The kinetic parameters, which are helpful for the prediction of adsorption rate, give important information for designing and modeling the adsorption processes (Santhi & Smitha 2010). Thus, the kinetics of AO67 dye adsorption onto MNC and MMNC was analyzed using pseudo-first-order, pseudo-second-order and Intraparticle diffusion, kinetic models. The conformity between experimental data and the model-predicted values was expressed by the correlation coefficients. The relatively higher value is the more applicable model to the kinetic of the dye ad-sorption onto the adsorbent.

Pseudo first - order kinetic model assumes that the rate of change of solute uptake with

time is directly proportional to difference in saturation concentration and the amount of solid uptake with time (Lagergran *et al.* 1998). The rate constant of adsorption is expressed as a first – order rate expression given as:

$$\ln (q_e - q_t) = \ln q_e - k_1 t \quad (6)$$

$q_e$  the concentration of AO67 adsorbed onto (MNC and MMNC) after equilibrium,

$q_t$  the concentration of AO67 adsorbed onto (MNC and MMNC) adsorbed in time  $t$ ,

$k_1$  ( $\text{min}^{-1}$ ) is pseudo 1st order rate constant.

The plot of  $\log (q_e - q_t)$  versus  $t$  should give a straight line with slope of  $-k_1/2.303$  and intercept  $\log q_e$  which allows calculation of adsorption rate constant  $k_1$  and equilibrium adsorption capacity  $q_e$ . The values of  $k_1$  and  $q_e$  were calculated for the adsorption of AO67 dye on (MNC and MMNC) at three of dye concentrations 50, 100 and 150 mg/L with constant temperature 25°C and calculated values of  $k_1$  and  $q_e$  at different temperatures 25, 40, 60 °C with constant dye concentration 100 mg/L, The results are summarized in Table 3. The pseudo first-order kinetic model of Lagergren does not fit well with the experimental data over the whole range of initial concentrations studied. The pseudo-second-order equation based on adsorption equilibrium capacity may be expressed in the form:

$$\frac{t}{qt} = \frac{1}{k_2 q_e^2} + \frac{t}{q_e} \quad (7)$$

Where,  $k_2$  ( $\text{g mg}^{-1} \cdot \text{min}^{-1}$ ) is the rate constant of pseudo-second-order adsorption and  $q_e$  is the equilibrium adsorption capacity ( $\text{mg/g}$ ). To understand the applicability of the models linear plots of  $t/q_t$  versus  $t$  at different AO67 dye concentrations (5, 100 and 150 mg/L) for adsorption onto MNC and MMNC have been plotted, and the results are presented in Figures 16(a,b and c). It was mentioned that the plot of  $t/q_t$  versus  $t$  gives relatively a straight line as showed in Figures (16 a,b and c), confirming the applicability of the pseudo-second-order equation. Values of  $k_2$  and equilibrium adsorption capacity  $q_e$  were calculated from the intercept and slope of the plots of  $t/q_t$  versus  $t$ , respectively. The values of

correlation coefficients  $R^2$ , for the pseudo-second-order kinetic model were found to be between (0.979 and 0.999) as presented in Table (4). This indicates that the adsorption system of MNC and MMNC obeys the pseudo-second-order kinetic model for the entire adsorption period, based on the assumption that the rate-limiting step may be chemisorptions involving valence forces through sharing or exchange of electrons between the adsorbent and adsorbate molecules (Mafra & Ferreira, 2013). It is evident from Tables (4), that the experimental data can be explained by the pseudo second order kinetics model, also  $q_e$ , calculated values are approximately equal to  $q_e$ , experimental values. The rate constant for pseudo second order kinetics decreases with increase in adsorbate concentration.

Intraparticle diffusion model: The time dependent data from this study was further used to investigate whether intra-particle kinetics also played significant roles in the adsorption of AO67 ions from their aqueous solutions (Rajeswari, *et al.* 2017). The intra-particle diffusion kinetic plots of  $q_t$  against  $t^{1/2}$  for AO67 was taken and presented in Figures (17 a, b and c). To investigate if intra-particle diffusion was the sorption rate limiting step, the Weber-Morris plot of  $q_t$  versus  $t^{1/2}$  was taken equation:

$$q_t = k_{id} t^{1/2} + c \quad (8)$$

where  $k_{id}$  is the intra-particle diffusion rate constant ( $\text{mg/g min}^{1/2}$ ) and  $C$  ( $\text{mg/g}$ ) is a constant that gives an idea about the thickness of the boundary layer; it was observed that the larger the value of  $C$  the greater the boundary layer effect (Dhakshinamoorthy, *et al.* 2012)

Comparing the  $k_{id1}$  values for the macropore and micropore diffusion stages for AO67 ions show that the rate limiting step is the micropore diffusion stage. This is because the micropore diffusion constant  $k_{id2}$  value for AO67 ions was lower than those for the macropore diffusion constants  $k_{id1}$ . This shows that the rate of micropore diffusion is the slower step and the rate determining step. The boundary layer effect i.e. the intercepts of the second lines from the plots in Figures (17 a, b

and c), was also presented in Table (3 and 4), which further shows greater effect at the micropore diffusion stage than at the macropore stage at different temperatures.

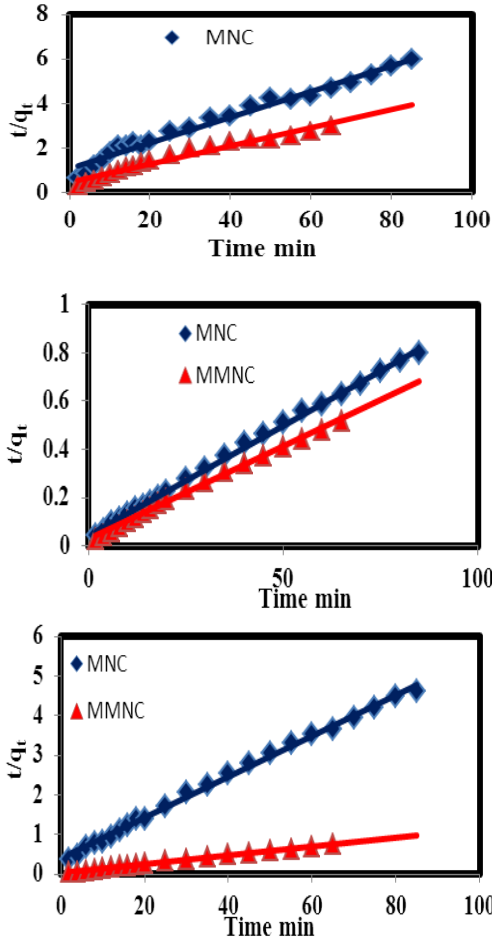


Figure (16): Pseudo-second-order kinetic for adsorption of the AO67 dye at concentration(a) 50 mg/L, (b) 100 mg/L and (c) 150 mg/L of AO67 onto MNC and MMNC.

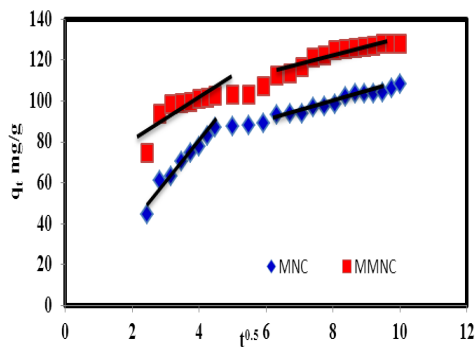


Figure (17a): Intraparticle Diffusion at temperature 25°C by (MNC and MMNC).

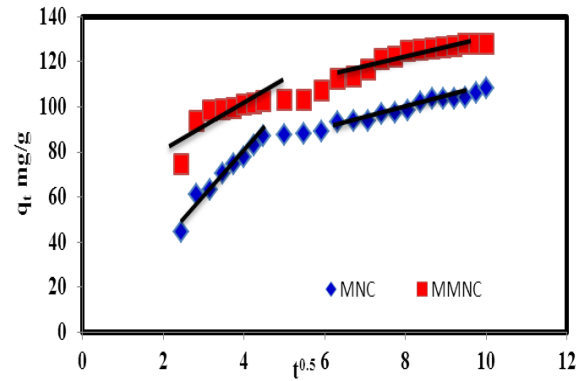


Figure (17b): Intraparticle Diffusion at temperature 40°C by (MNC and MMNC).

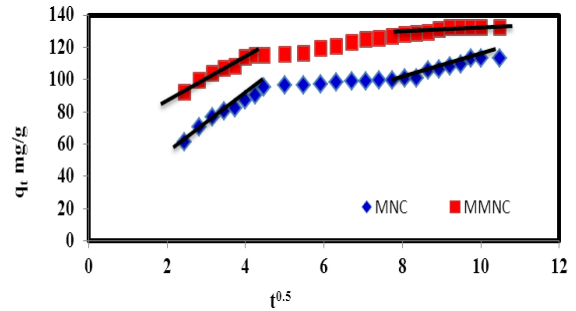


Figure (17c): Intraparticle Diffusion at temperature 60°C by (MNC and MMNC).

### 3.5. Removal of the dyes from textile wastewaters

Under optimum conditions which attained in this study for removal of AO67 onto MMNC from aqueous solution, removal of (RB222, RY145 and AR37) was studied from the simulated wastewaters onto MMNC. The low and the high amount of adsorbent, contact time, the capacity of adsorbents and removal percentages were considered in the simulated wastewaters. Fig. (18 and 19) represent the effect of contact time on removal % and adsorbent capacity. The Figures show the removal of different dyes (RB222, RY145, AO67 and AR37) from wastewaters may be carried out by using MMNC under optimum conditions, the effect of adsorbent more affective for dye (AR37) than dye (RB222, RY145, AO67).

**Table (2): Summarize the Langmuir, Freundlich, Temkin and D-R Isotherm isotherm models constants and correlation coefficients for adsorption of AO67 dye onto MNC and MMNC at different temperatures.**

Adsorbents	parameter Temp. (°C)	Langmuir Isotherm				Freundlich Isotherm			Temkine			D-R Isotherm	
		$k_L$ (L/mg)	$q_m$ (mg/g)	$R_L$	$R^2$	$k_f$ (L/mg)	N	$R^2$	a	b	$R^2$	$q_{D-R}$ mg/g	$R^2$
MNC	25	0.009	156.25	0.307-0.956	0.9717	1.7	1.2	0.9188	6.33	82.32	0.7211	60.63	0.7187
	40	0.0135	158.73	0.219- 0.933	0.9922	3.8	1.48	0.933	3.76	60.79	0.8615	69.048	0.5959
	60	0.0154	161.29	0.204-0.927	0.9336	4.7	1.54	0.9407	5.29	81.03	0.8695	75.42	0.6145
MMNC	25	0.0132	163.93	0.206- 0.928	0.9022	3.73	1.4	0.8662	4.89	72.8	0.9397	86.93	0.8311
	40	0.0139	222.22	0.232- 0.938	0.9763	6.72	1.61	0.9578	5.07	62.5	0.9624	96.69	0.6726
	60	0.0162	243.9	0.238- 0.939	0.9795	7.4	1.62	0.9667	5.22	60.5	0.9606	103.29	0.6292

**Table (3): Summarize the kinetics model constants and correlation coefficients for adsorption of AO67 dye onto MNC and MMNC at different temperatures.**

Adsorbent	Temp °C	Pseudo first order			Pseudo second order						Intraparticle diffusion model			
		$k_1$ min <sup>-1</sup>	$q_e$ (cal) mg/g	$R^2$	$k_2$ g mg <sup>-1</sup> min <sup>-1</sup>	$q_e$ (exp.) mg /g	$q_e$ (cal.) mg /g	H	NSD	$R^2$	$k_1$ mg/g min <sup>1/2</sup>	$R^2$	$k_2$ mg/g min <sup>1/2</sup>	$R^2$
MNC	25	0.0263	28.11	0.4176	$1.92 \times 10^{-3}$	<b>107.2</b>	109.89	23.19	1.45	0.9984	16.68	0.9306	3.5518	0.964
	40	0.0274	40.5	0.9202	$2.39 \times 10^{-3}$	<b>112.24</b>	111.11	29.5	0.58	0.9977	14.36	0.9465	3.389	0.9479
	60	0.033	43.95	0.8422	$2.52 \times 10^{-3}$	<b>113.29</b>	112.36	31.81	0.47	0.998	11.898	0.9203	3.469	0.8463
MMNC	25	0.0371	48.7	0.9836	$2.28 \times 10^{-3}$	<b>126.93</b>	129.87	38.45	0.9	0.9986	10.64	0.6667	3.3696	0.8604
	40	0.041	50.75	0.09496	$2.75 \times 10^{-3}$	<b>130.34</b>	131.58	47.61	1.25	0.999	7.59	0.912	2.417	0.9124
	60	0.0433	44.14	0.09597	$3.45 \times 10^{-3}$	<b>132.32</b>	133.33	61.33	0.134	0.9992	6.4798	0.9655	1.64	0.9917

**Table (4): Summarize the kinetics model constants and correlation coefficients for adsorption of AO67 dye onto MNC and MMNC at different concentration.**

Adsorbent	Conc. mg/L	Pseudo first order			Pseudo second order						Intraparticle diffusion model			
		$k_1$ min <sup>-1</sup>	$q_e$ (cal) mg/g	$R^2$	$k_2$ g mg <sup>-1</sup> min <sup>-1</sup>	$q_e$ (exp.) mg /g	$q_e$ (cal.) mg /g	H	NSD	$R^2$	$k_1$ mg/g min <sup>1/2</sup>	$R^2$	$k_2$ mg/g min <sup>1/2</sup>	$R^2$
MNC	50	0.029	13.52	0.9248	$3.14 \times 10^{-3}$	14.27	17.27	0.937	12.14	0.979	1.634	0.921	1.2335	0.6017
	100	0.0361	47.24	0.9651	0.0193	107.20	109.89	233.06	1.45	0.9984	14.721	0.9753	1.5479	0.6441
	150	0.03	10.46	0.9688	$5.24 \times 10^{-3}$	18.93	19.92	2.08	3.02	0.9968	5.4578	0.7052	0.6266	0.7938
MMNC	50	0.04	17.74	0.9594	$3.45 \times 10^{-3}$	21.8	24.57	2.083	6.74	0.9813	1.5143	0.9427	0.6967	0.5684
	100	0.054	55.72	0.9819	0.023	126.93	129.87	387.92	1.34	0.9989	7.8381	0.9655	1.4758	0.5809
	150	0.041	31.57	0.9304	$6.99 \times 10^{-3}$	88.64	90.91	57.77	1.48	0.9979	2.6866	0.9234	0.2754	0.5607

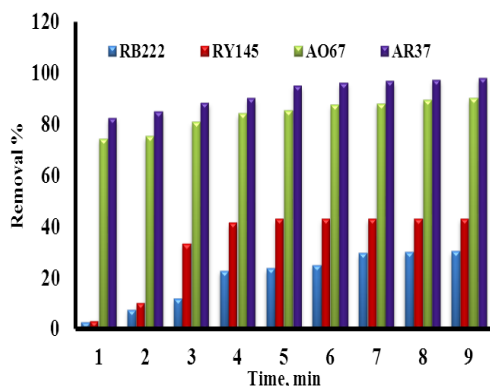


**Figure (18):** Effect of contact time on removal % of RB 222, RY 145, AO67 and AR37 by MMNC at optimum condition.

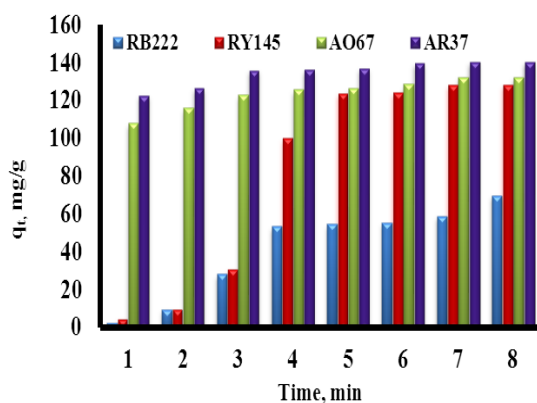


**Figure (19):** Effect of contact time on  $q_t$  of RB 222, RY 145, AO67 and AR37 by MMNC at optimum condition.

#### 4. CONCLUSION

1. Synthesis of mixed nano-composite of iron oxide and alumina and modified by cationic surfactant CTAB generates a porous surface with high surface area which is suitable for the adsorption of AO67 dye.
2. The results of batch experiments for removal of AO67 showed that the adsorption capacity increased with increasing the contact time and the initial pH of AO67 solutions with maximum adsorption capacity at pH 5.5 of MNC and pH 8.5 of MMNC. However, the adsorption capacity decreased with increasing mass of the adsorbent.
3. Kinetic data of adsorption are well fitted by the pseudo 2nd order kinetic model with a good agreement with the intra-particle diffusion model.
4. The equilibrium experimental data fits perfectly the Langmuir isotherm which implies the

monolayer formation on the surface of MNC and MMNC.

6. The optimum conditions which attained in this study for removal of AO67 onto MMNC from aqueous solution, removal of (RB222, RY145 and AR37) was studied from the simulated wastewaters onto MMNC.
7. The results show the removal of different dyes (RB222, RY145, AO67 and AR37) from wastewaters may be carried out by using MMNC under optimum conditions, the effect of adsorbent more affective for dye (AR37) than dye (RB222, RY145, AO67).

#### 5. REFERENCE:

- Aharoni C. and Sparks D. L. (1991):** Kinetics of Soil Chemical Reactions-A Theoretical Treatment. In: D. L. Uarez (Eds.). Rate of Soil Chemical Processes, Soil Science Society of America. Madison, WI. 1:18.
- Alvarez C. M., Zilkova N., Pariente J. P. and Cejka J. (2008):** Synthesis, Characterization and Catalytic applications of organized mesoporous aluminas. *J. Catalysis Reviews*; Vol. 50, 222:286.
- Arshak K. and Gaidan I. (2005):** Development of a noble gas sensor based on oxides thick films. *J. Mater. Sci. Eng. B*; Vol. 118, 45:49.
- Akazdam S., Chafi M., Yassine W. and Gourich B. (2017):** Removal of Acid Orange 7 Dye from Aqueous Solution Using the Exchange Resin Amberlite FPA-98 as an Efficient Adsorbent: Kinetics, Isotherms, and Thermodynamics Study. *J. Mater. and Enviro. Sci*; Vol. 8, 2993:3012.
- Bajpai S. K. and Jain A. (2010):** Sorptive Removal of Crystal Violet from Aqueous Solution Using Spent Tea Leaves: Part I Optimization of Sorption Conditions and Kinetic Studies. *J. Act. Chim. Slov*; Vol. 36, 57: 751.
- Bajpai S. K. and Jain A. (2012):** Equilibrium and thermodynamic studies for adsorption of crystal violet onto spent tea leaves. *J. Water S.A*; Vol. 4, 221:228.
- Bhattacharyya K.G. and Sharma A. (2005):** Kinetics and mechanism of removal of methylene blue by adsorption on various carbons-a comparative study. *J. Dyes and pigments*; Vol. 51, 25:40.
- Dakhil I. S. (2013):** Adsorptive removal of dye from industrial effluents using natural iraqi

- palygorskite clay as low-cost adsorbent. *J. Asian Scientific Research*; Vol. 3, 945:955.
- Dhakshinamoorthy A., Alvaro M. and Garcia H. (2012):** Aerobic oxidation of cycloalkenes catalyzed by iron metal organic framework containing N-hydroxyphthalimide. *J. Catal*; Vol. 289, 259:265.
- Faraji M., Yaminiand Y., Rezaee M. (2010):** Magnetic Nanoparticles: Synthesis, Stabilization, Functionalization, Characterization, and Applications. *J. Iran. Chem. Soc*; Vol. 7, 1:37.
- Gupta V. (2009):** Application of low-cost adsorbents for dye removal—a review. *J. Environ Manage*; Vol. 42, 908:2313.
- Hashemian S. (2010):** MnFe<sub>2</sub>O<sub>4</sub> / bentonite nano composite as a novel magnetic material for adsorption of acid red 138. *J. African Biotechnology* Vol. 9, 8667:8671.
- Hamid A. S., Parastoo D. and Ahmad M. (2016):** Adsorptive Removal of Reactive Orange 122 from aqueous solutions by ionic liquid coated Fe<sub>3</sub>O<sub>4</sub> magnetic nanoparticles as an efficient adsorbent. *J. Iran. Chemistry Chemical Engineering*; Vol. 35, 63: 73.
- Kant R. (2012):** Adsorption of dye eosin from an aqueous solution on two different samples of activated carbon by static batch method. *J. Water Resour Prot*; Vol. 8, 4:93.
- Karami H. (2010):** Investigation of sol-gel Synthesized CdO-ZnO Nanocomposite for CO Gas Sensing, *Int. J. Electrochem. Sci*; Vol. 5, 720 : 730.
- Kim S.M., Lee Y.J., Jun K.W., Park J.Y. and Potdar H.S. (2007):** Synthesis of thermo-stable high surface area alumina powder from sol-gel derived boehmite. *J. Materials Chemistry and Physics*; Vol. 104, 56:61.
- Langmuir I. (1916):** The constitution and fundamental properties of solids and liquids. *J. American Chemical Society*; Vol. 38, 2221:2295.
- Lagergran S.,Sven K., Hand V.,(1998):**Thermodynamic and Dynamic of Chromium Biosorption by Pectic and Lignocellulocic Biowastes. *J. Water Resource and Protection*. Vol. 24, 1:39.
- Mafra, I.M. Z. and Ferreira, M. A. (2013):** Adsorption of remazol brilliant blue on an orange peel adsorbent. *Brazilian. J. Chemical Engineering*; Vol. 30, 657: 665.
- Muntean S.G. , Nistor M.A, Muntean E., Todea A., Ianos R. and Pscurariu C.(2018):** Removal of Colored Organic Pollutants from Wastewaters by Magnetite/Carbon Nanocomposites: Single and Binary Systems. *J. of Chemistry, Hindawi Article ID 6249821,1: 16*
- Nalwa H.S. (2009):** Encyclopedia of Nanoscience and Nanotechnology. *J. American scientific publishers*; Vol.8, 340:346.
- Patil U. L. (2014):** Removals of Sudan Red G dye from aqueous solution by adsorption on to activated carbon prepared from mosambi and cotton an agricultural waste.*J. International Science, Environment and Technology*; Vol. 3, 546:555.
- Rouf S., Nagapadma M. and Ramakoteswara R. (2015):**Removal of Harmful Textile Dye Congo Red from Aqueous Solution Using Chitosan and Chitosan Beads Modified with CTAB. *J. Int. Engineering Research and Applications*; Vol. 5, 75:82.
- Rajabi A.A., Yamini Y., Faraji M. and Nourmohammadian F. (2016):**Modified magnetite nanoparticles with cetyltrimethylammonium bromide as superior adsorbent for rapid removal of the disperse dyes from wastewater of textile companies. *J. Nano. Chem. Res*; Vol. 1, 49:56.
- Rajeswari K. M., Revanth T., Anirudh A. and Prasad B. (2017):**Removal of Crystal Violet dye from aqueous solution using water hyacinth: Equilibrium, kinetics and thermodynamics study. *J. Resource-Efficient Technologies*; Vol. 3, 71:77.
- Santhi M. and Smitha. (2010).** Removal of methyl red from aqueous solution by activated carbon prepared from the annona squmosa seed by adsorption. *Chemical Engineering J. Int. of Innovative Research in Science Engineering and technol.* Vol. 4, 497:510.
- Seeds S. B. (2011):** Removal of Orange 7 Dye from Wastewater Used by Natural Adsorbent of Moringa Oleifera.*J. American Environmental Engin*; Vol. 1, 1:9.
- Sen T.K., Afroze S. and Ang H. (2011):**Equilibrium, kinetics and mechanism of removal of methylene blue from aqueous solution by adsorption onto pine cone biomass of Pinus radiate.*J. Water Air Soil Pollut*; Vol. 515, 218:499.
- Srivastava V., Weng C. H., Singh V. K. and Sharma Y. C. (2011):** Adsorption of nickel ions from aqueous solutions by nano alumina: kinetic, mass transfer, and equilibrium studies. *J. Chemical & Engineering Data*; Vol. 56, 1414:1422.

- Tsai W. T., Chang Y. M., Lai C. W. and Lo C. C. (2005):** Adsorption of ethyl violet dyes in aqueous solution by regenerated spent bleaching earth. *J. Colloid and Interface Science*; Vol. 289, 322:333.
- Ventra M.D., Evoy S. and Heflin J.R. (2004):** Introduction to Nanoscale Science and Technology. *J. Springer*; 199: 208.
- Yagub M.T., Sen T.K. and Ang H. (2012):** Equilibrium, kinetics, and thermodynamics of methylene blue adsorption by pine tree leaves. *J. Water Air Soil Pollut*; Vol. 82, 2238:5267.
- Yu C., Dong X., Guo L., Li J., Qin F., Zhang L., Shi J. and Yan D. (2008):** Template-Free Preparation of Mesoporous Fe<sub>2</sub>O<sub>3</sub> and Its Application as Absorbents, *J. Phys. Chem. C*; Vol. 112, 13378:13382.

## الملخص العربي

تم تحضير خليط من المركبات النانوية لأوكسيد الحديد / الألمنيوم (Fe<sub>2</sub>O<sub>3</sub>- Al<sub>2</sub>O<sub>3</sub>) بالطريقة الحرارية المائية وتم تحويل شكلها باستخدام الـ CTAB السطحي الكاتيوني لإزالة الصبغة الحامضية البرتقالية ٦٧ واجري على المادتين التي تم الحصول عليها الوصف المورفولوجي وحجم المترابكات النانوية مثل SEM و EDX و TEM. وأيضا اجري على المركبات الناتجة استخدام XRD و FT-IR. وأجريت تجارب الامتزاز الدفعي لإزالة الصبغة الحمضية AO67 من محلول مائي. تمت دراسة امتزاز AO67 على المركبات النانوية الناتجة وتم دراسة تأثيرات مختلفة مثل تأثير تركيز CTAB ، تأثير محلول الصبغة الهيدروجينية ، تأثير التركيزات المختلفة للصبغة ، كتلة المادة المازة تأثير الوقت على قدرة الامتصاص. تم تقييم قدرات الامتزاز باستخدام نماذج Langmuir و Freundlich Dubinin- Radushkevich (D-R) و Tekmin isotherm ، ووجد ان النتائج التجريبية للتوازن تناسب تماما مع Langmuir. تم تحليل البيانات الحركية الدفعية باستخدام النماذج الحركية من الدرجة الأولى والثانية الكاذبة، وغيرها من النماذج الحركية المختلفة. تم تزويد البيانات الحركية للامتزاز بشكل جيد عن طريق النموذج الحركي الكاذب من الدرجة الثانية مع اتفاق جيد مع نموذج الانتشار داخل الجسيم. ولهذا يمكن اعتبار المركب النانوي المحضر كمتص محتمل لإزالة AO67 في معالجة مياه الصرف الصحي. واستخدمت الظروف المثلى للتطبيق في إزالة صبغات مياه الصرف لهذه الصبغات (RB222 و AR37 و RY145).